**Electronic Supplementary Information (ESI) for**

# Strongly coupled ultrasmall-$Fe_7C_3$/N-doped porous carbon hybrids for high efficient Zn-air batteries

Lulu Chen,[a,b] Yelong Zhang,[c] Xiangjian Liu,[a,b] Ling Long,[a,b] Siyu Wang,[a,b] Wenxiu Yang *[c] and Jianbo Jia *[a,b,d]

[a] State Key Laboratory of Electroanalytical Chemistry, Changchun Institute of Applied Chemistry, Chinese Academy of Science, Changchun 130022, China.

[b] University of Science and Technology of China, Hefei 230026, China.

[c] Department of Materials Science & Engineering & Department of Energy and Resources Engineering, College of Engineering, Peking University, Beijing 100871, China.

[d] School of Biotechnology and Health Sciences, Wuyi University, Jiangmen 529020, China.

* Corresponding author

Tel & Fax: (+86)-431-85262251

E-mail: jbjia@ciac.ac.cn

## Experimental Section

*Chemicals and Characterizations:* We bought dopamine and 2-amino-2-hydroxymethylpropane-1,3-dio (Tris) from Aladdin. We bought PEG-PPG-PEG (P123, Mw = 5800) and Nafion (5.0 wt %) from Sigma-Aldrich. We bought $Zn(Ac)_2$, triethanolamine, iron nitrate hexahydrate, and $N_2H_4$ (5 wt %) from Beijing Chemical Reagent Co. Ltd. We bought Pt/C (20 wt %) from Johnson Matthey. A Bruker D8 ADVANCE instrument was employed to obtain the X-ray diffraction patterns of the prepared samples. The morphology characterizations and corresponding elemental mapping images were taken out on a FEI TECNAI $G^2$ high resolution microscope. X-Ray photoelectron spectroscopy (XPS) analysis was obtained from ESCALAB 250. Thermogravimetric analysis (TGA) of samples was obtained from NETZSCH STA 449F3. Raman spectra were measured by a Renishaw 2000 model confocal microscopy. Nitrogen adsorption-desorption isotherms were performed on an ASAP 2020 Physisorption Analyzer. Inductively couple plasma-optical emission spectrometer (ICP-OES) was taken on a PerkinElmer ICP instrument. Electrochemical impedance spectroscopy (EIS) was record on a CHI660E electrochemical workstation. And CHI842B electrochemical workstation was utilized to perform the rotating ring-disk electrode (RRDE) curves and cyclic voltammetry (CVs) measurements. X-ray absorption near-edge structure (XANES) and extended X-ray absorption fine structure (EXAFS) measurements were carried out at 1W2B end station, Beijing Synchrotron Radiation Facility (BSRF).

*Electrochemical measurements:* All of the electrochemical experiments were conducted by a three-electrode system. The catalysts were modified on the glassy carbon electrode (GCE), which was employed as the working electrode. The Ag/AgCl (saturated KCl) electrode and graphite rod were used as the reference and the counter electrode, respectively. The potential against the Ag/AgCl electrode was converted into the potential against the reversible hydrogen electrode (RHE) by the following equation: E(vs. RHE) = E(vs. Ag/AgCl) + 0.059pH + 0.197. To obtain the homogeneous ink (2 mg $mL^{-1}$) of the catalyst, a certain mass of catalyst was added into the mixed solution of isopropyl, water, and Nafion with a certain ratio (1:20:0.075) of the volume. After the sufficient ultrasonication, the ink was passed onto the GCE with the dosage of 1000 μg $cm^{-2}$. And the loading dosage of the commercial Pt/C is 25 μg Pt $cm^{-2}$. Cyclic voltammetry (CV) with different scan rates of 1, 2, 4, 6, 8, and 10 mV $s^{-1}$ were recorded to calculate the electrochemical double layer capacitances ($C_{dl}$) of the samples. A simplified equivalent circuit was applied to suit the curves in the electrochemical impedance spectroscopy (EIS) measurements, which were obtained in the range of frequencies from 100 Hz to 0.01 kHz. To obtain the RRDE curves in 0.10 M KOH, the potential of the disk and the ring were both set at 1.064 V. The scan rate is 5 mV $s^{-1}$ and the rotation rate is 1600 rpm. The electron transfer number (n) and $H_2O_2$ yield ($H_2O_2$%) were figured out by the RRDE characterizations with the equations:

$$H_2O_2\% = \frac{200\frac{I_r}{N}}{I_d + \frac{I_r}{N}} \quad (1)$$

$$n = \frac{4I_d}{I_d + \frac{I_r}{N}} \quad (2)$$

N is the current collection efficiency, which is measured to be 0.44 by utilizing $[Fe(CN)_6]^{4-}/[Fe(CN)_6]^{3-}$ redox couple. $I_d$ and $I_r$ are the current on the ring electrode and disk electrode, respectively.

Linear sweep voltammetry (LSV) curves were measured at a scan rate of 5 mV $s^{-1}$ and the rotation rate is 1600 rpm. The electron transfer number can be also calculated from the Koutecky-Levich equation:

$$\frac{1}{J} = \frac{1}{J_L} + \frac{1}{J_K} = \frac{1}{B\omega^{1/2}} + \frac{1}{J_K}$$

$$B = 0.62nFC_0(D_0)^{2/3}V^{-1/6}$$

where J is the measured current density, $J_K$ and $J_L$ are the kinetic and limiting current densities, ω is the angular velocity of the rotating disk, n is the electron transfer number, F is the Faraday constant (96485 C•$mol^{-1}$), $C_o$ is the bulk concentration of $O_2$ in 0.10 M KOH solution ($1.2 \times 10^{-6}$ mol•$cm^{-3}$), $D_o$ is the diffusion coefficient of $O_2$ ($1.9 \times 10^{-5}$ $cm^2$•$s^{-1}$), and V is the kinematic viscosity of 0.10 M KOH solution (0.01 $cm^2$•$s^{-1}$).

*Zn-air battery assembly:* The air cathode was first made by dropping a certain volume of catalyst inks onto a carbon paper substrate, and then dried overnight in a vacuum oven at 70°C. A homemade Zn-air battery was fabricated with a *u*-$Fe_7C_3$@NC-based cathode, a Zn foil anode, and an aqueous alkaline electrolyte (7 M KOH + 0.2 M $ZnCl_2$). Both the specific capacity and energy density values were

calculated based on the mass of consumed Zn during the discharge process. For comparison purposes, the commercial Pt/C structured battery was also tested. The loading mass was 0.1 mg $cm^{-2}$ for all materials. Galvanostatic tests of the assembled batteries were performed with a Land CT2001A battery test system.

*Preparation of Catalysts:*

Synthesis of ZnO nanospheres. The ZnO nanospheres were prepared by the ultrasonication method. First, 0.88 g of $Zn(Ac)_2$ and 6.02 g of triethanolamine were dissolved in 40 and 200 mL $H_2O$, respectively. The above two solution were mixed with stirring, and then ultrasonicated for 30 min to get a milk-like suspension. The suspension liquid was then aged at room temperature for 12 h, followed by centrifugation, washed for several times, and dried at vacuum environment overnight.

Synthesis of *u*-$Fe_7C_3$@NC. 100 mg of ZnO nanospheres was dispersed in 100 mL $H_2O$, which includes 0.12 g of Tris and 0.08 g of P123. Then, 40 mL distilled water containing 0.20 g of dopamine was poured into the above solution with stirring for another 2 h. After centrifugation and washing with ethanol, ZnO/DA was acquired. ZnO/DA was then dispersed in 10 mL $H_2O$ containing 1.0 mmol $Fe(NO_3)_2 \cdot 6H_2O$. After altrasonicating for 30 min, 5 mL of $N_2H_4$ (5%) was dropped into the above solution followed by stirring for 30 min. Fe/ZnO/DA was get by centrifugation, washed with water, and dried at 60 ºC. Finally, Fe/ZnO/DA was subsequently annealed with the protection of $N_2$ (900 ºC) for 2 h. The final product was obtained after immersed in 1.0 M HCl to remove the unstable particles. In addition,

Fe/ZnO/DA was pyrolysed at 500 and 700° C for 2 h to explore the formation process of *u*-$Fe_7C_3$@NC. For comparison, N-doped carbon (NC) was synthesized under the same conditions without $Fe(NO_3)_2 \cdot 6H_2O$. To understand the role of the ZnO template, Fe/DA was synthesized under the same conditions without ZnO nanospheres.

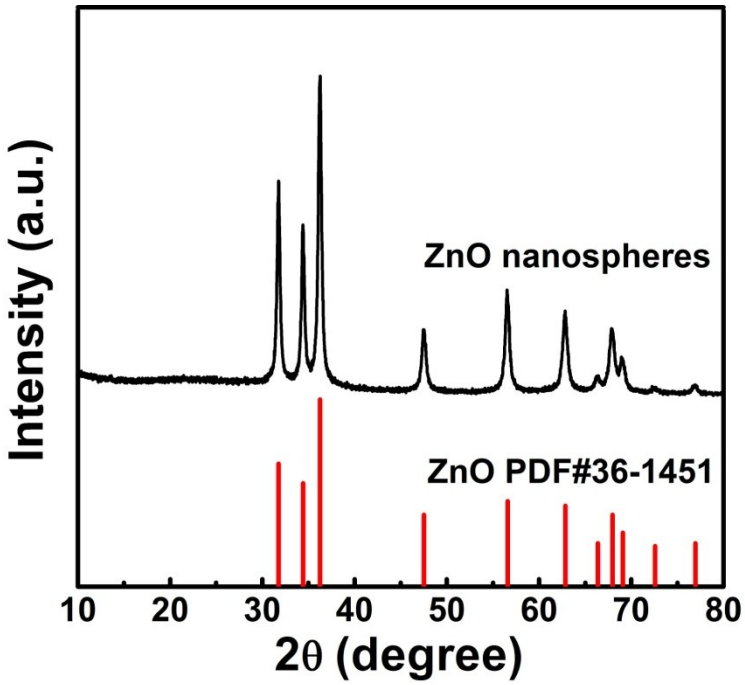


**Fig. S1** XRD pattern of ZnO nanospheres.

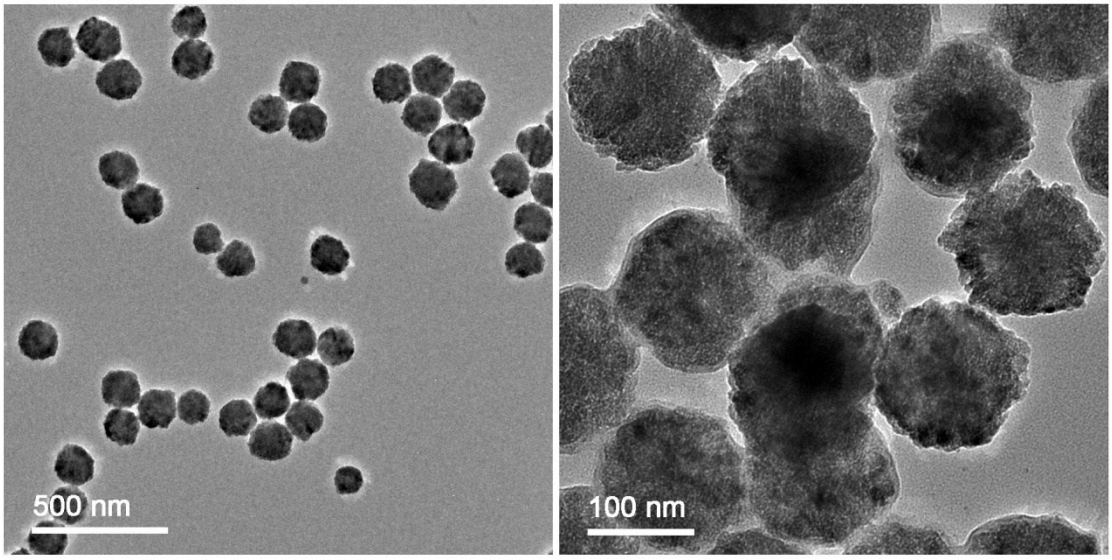


**Fig. S2** TEM images of ZnO nanospheres.

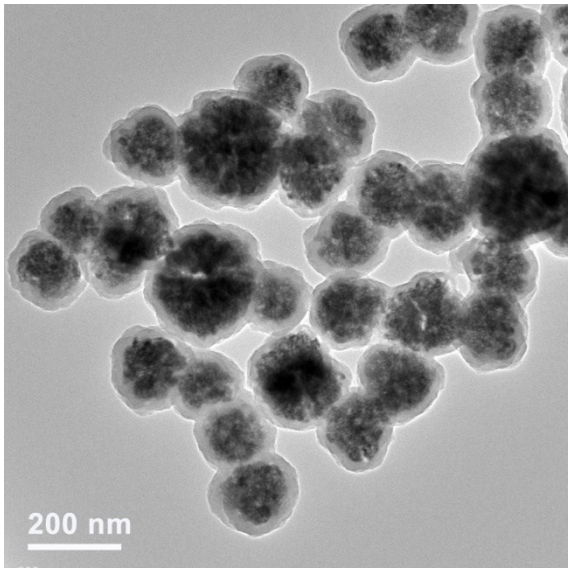


**Fig. S3** TEM image of ZnO/DA.

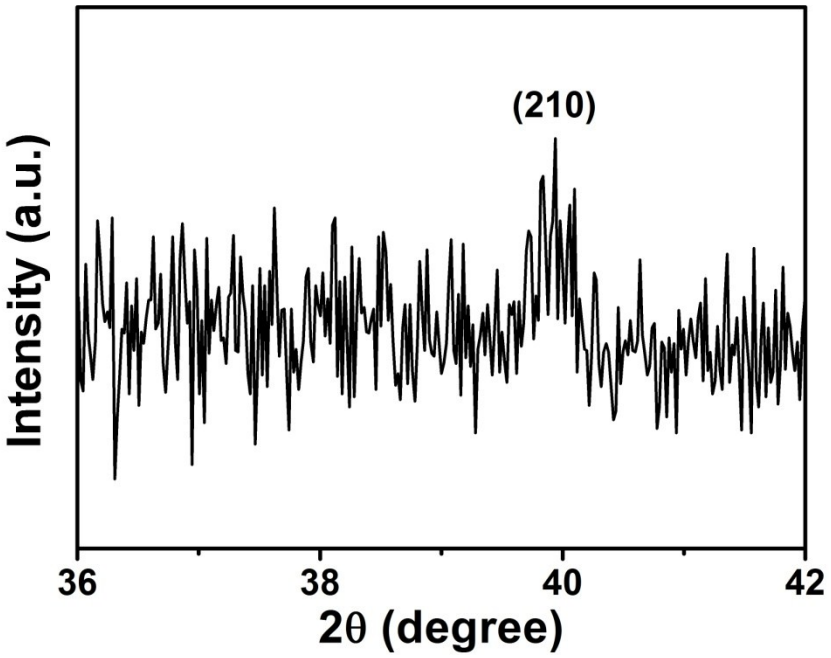


**Fig. S4** The enlarged XRD pattern of *u*-$Fe_7C_3$@NC from 36 to 42°. The peak at 40° is relatively weak due to the poor crystallinity.

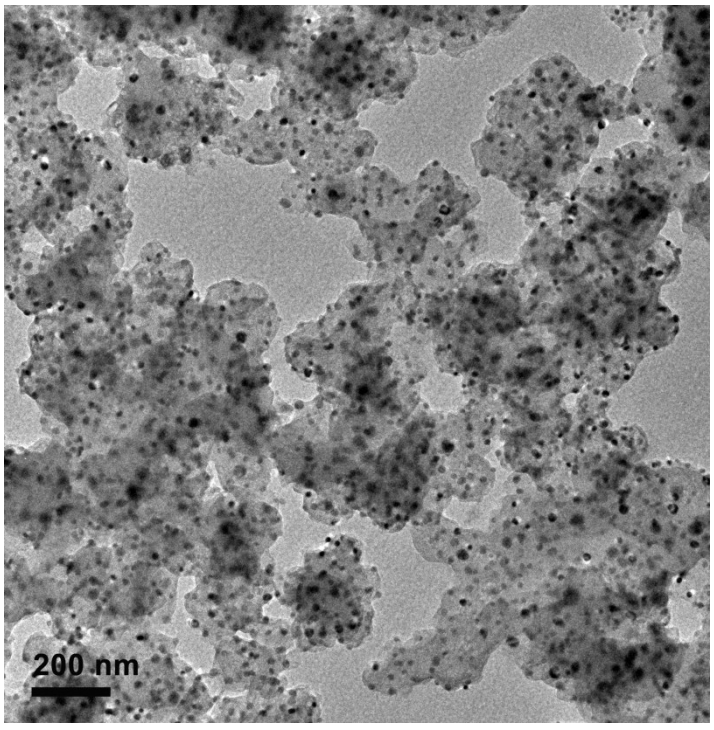


**Fig. S5** TEM image of *u*-$Fe_7C_3$@NC.

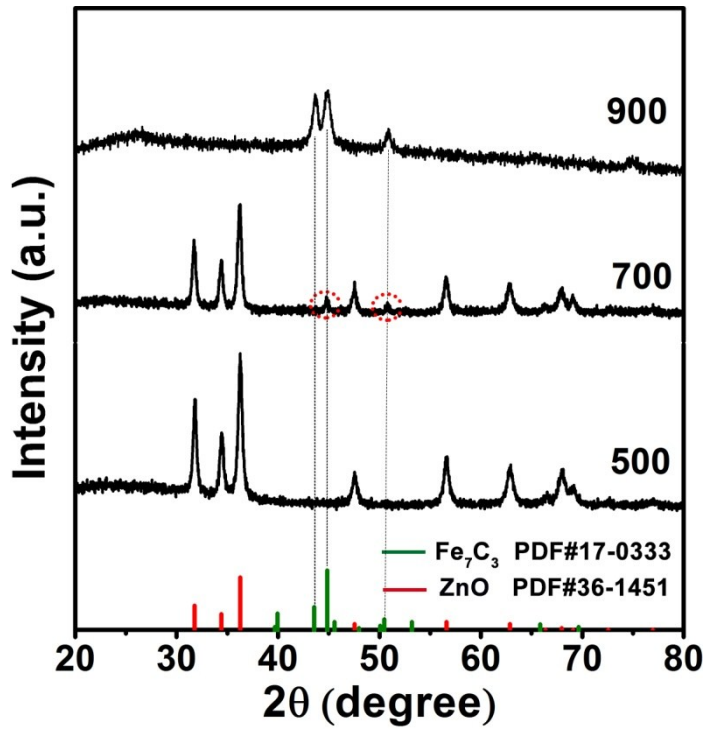


**Fig. S6** XRD patterns of samples pyrolyzed at 500, 700, and 900 ºC.

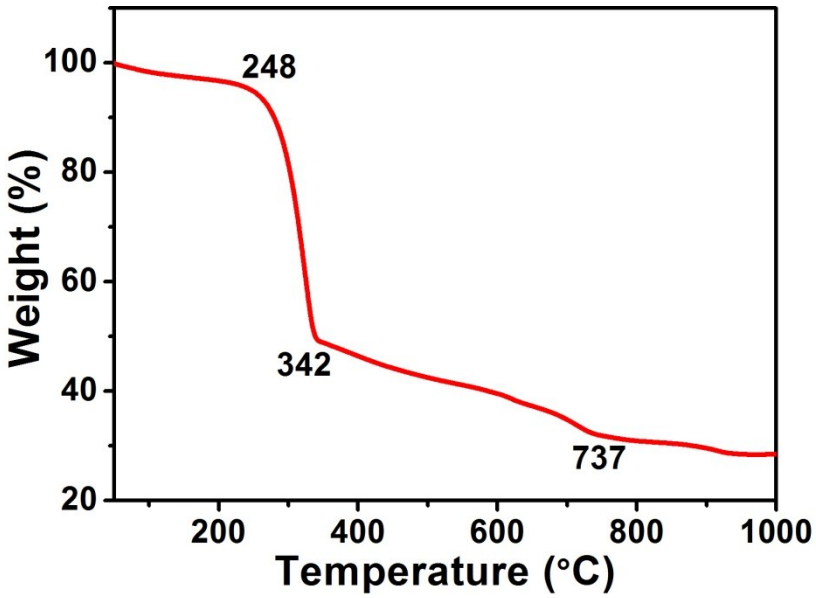


**Fig. S7** Thermogravimetric analysis (TGA) of Fe/ZnO/DA in $N_2$ atmosphere with a heating rate of 10 ºC $min^{-1}$.

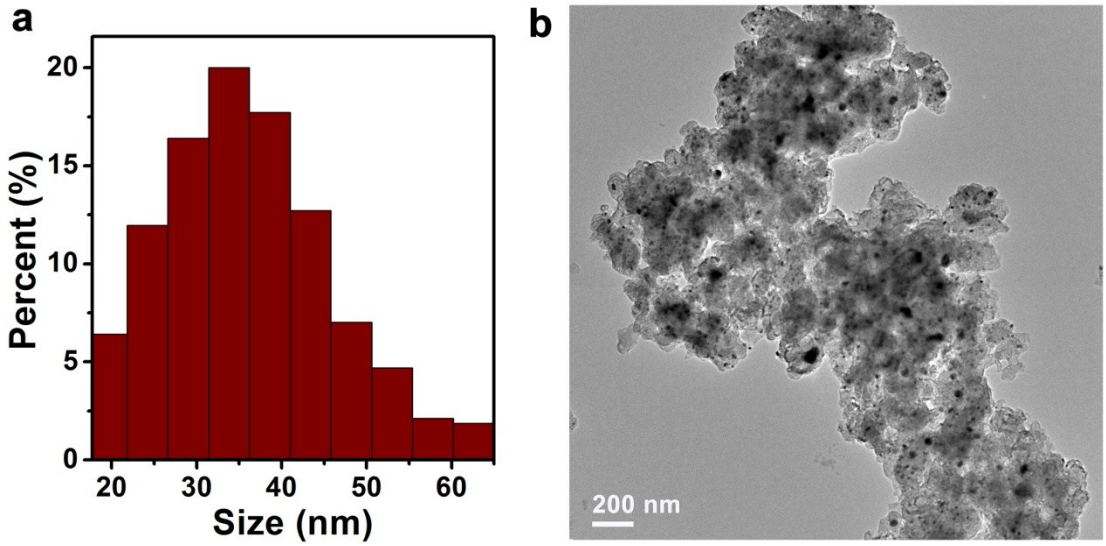


**Fig. S8** (a) The size statistical analysis of nanoparticles in Fe/DA. (b) TEM image of Fe/DA.

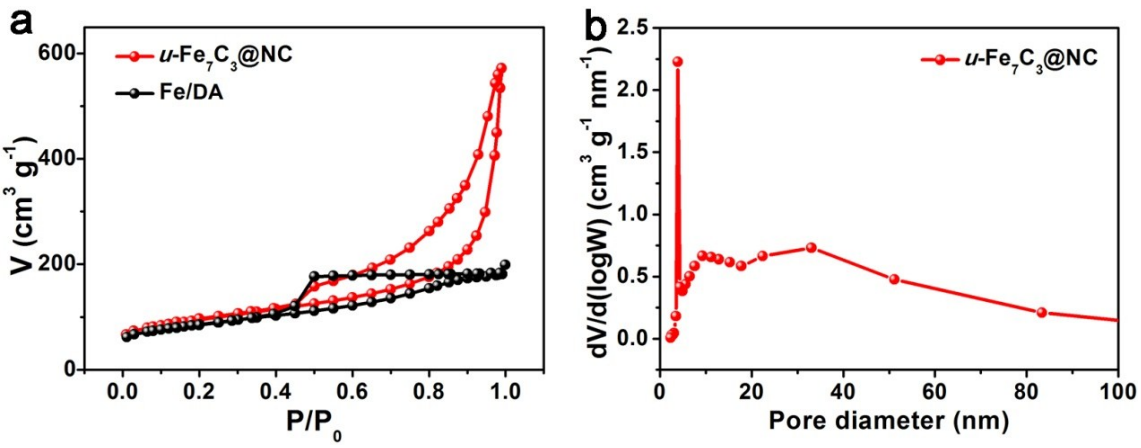


**Fig. S9** (a) $N_2$ adsorption-desorption curves of *u*-$Fe_7C_3$@NC and Fe/DA. (b) Pore distribution curve of *u*-$Fe_7C_3$@NC.

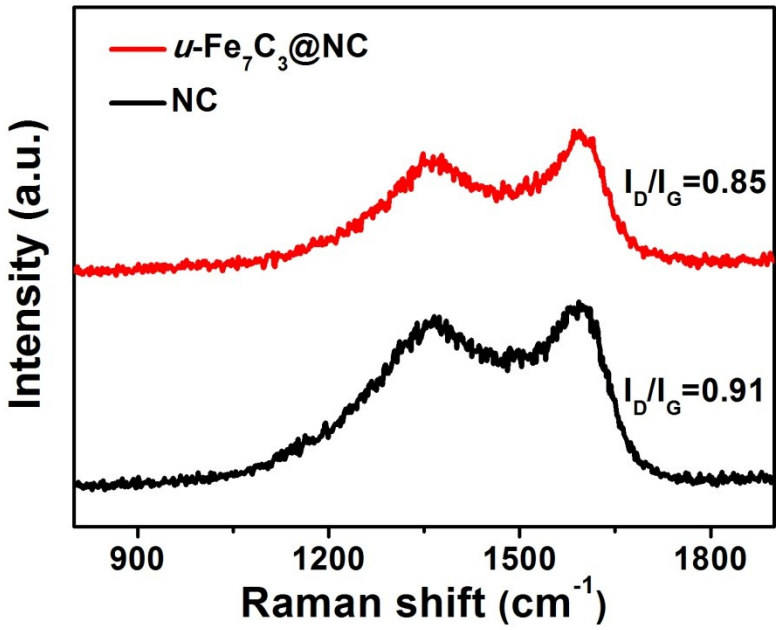


**Fig. S10** Raman spectra of *u*-$Fe_7C_3$@NC and NC.

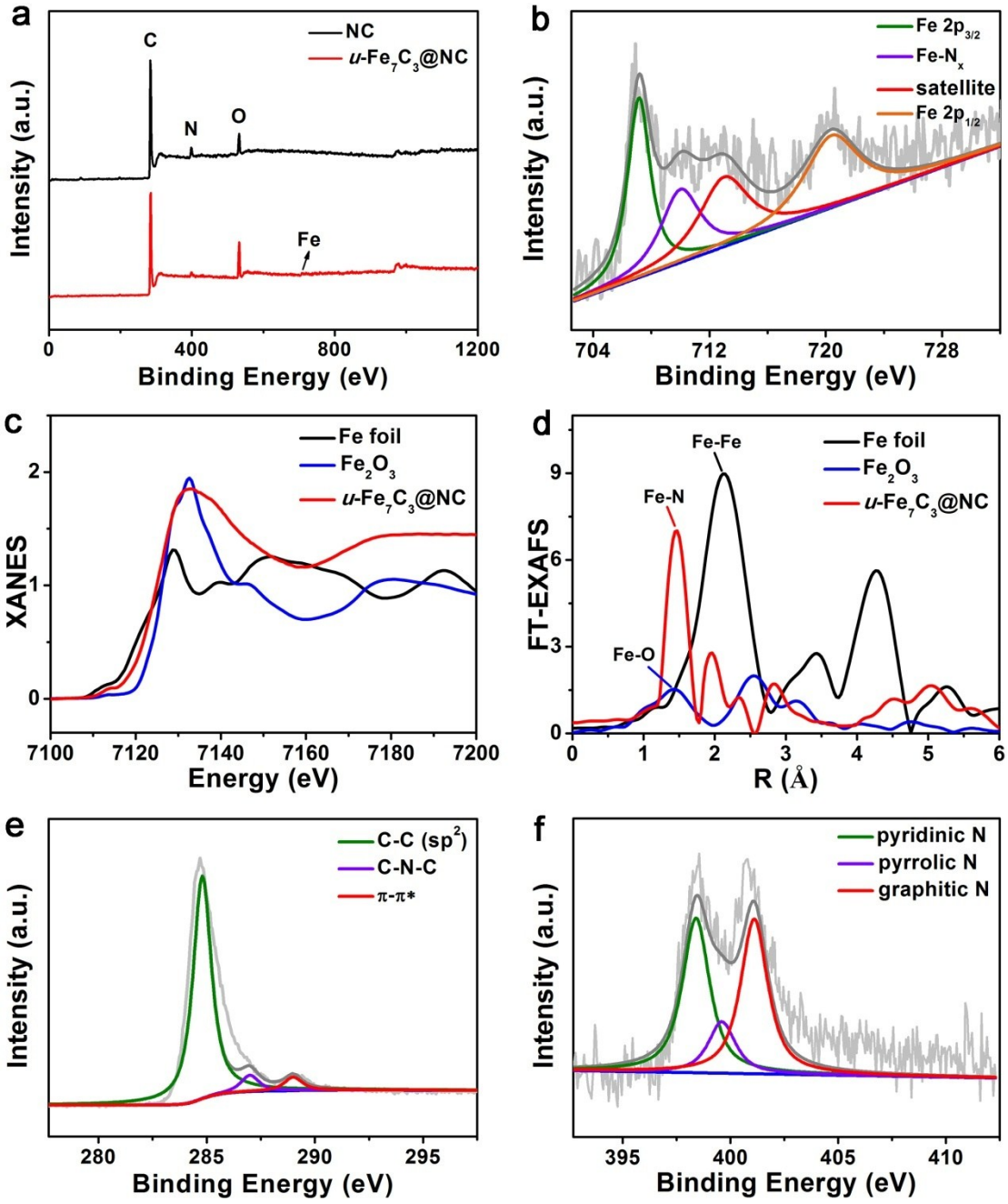


**Fig. S11** (a) XPS spectra of *u*-$Fe_7C_3$@NC and NC. (b) High resolution XPS spectra of Fe in *u*-$Fe_7C_3$@NC. (c) Fe K edge XANES spectra and (d) Fourier transforms of $k_3$-weighted Fe K-edge EXAFS spectra for Fe foil, $Fe_2O_3$, and *u*-$Fe_7C_3$@NC. High resolution XPS spectra of (e) C and (f) N in *u*-$Fe_7C_3$@NC.

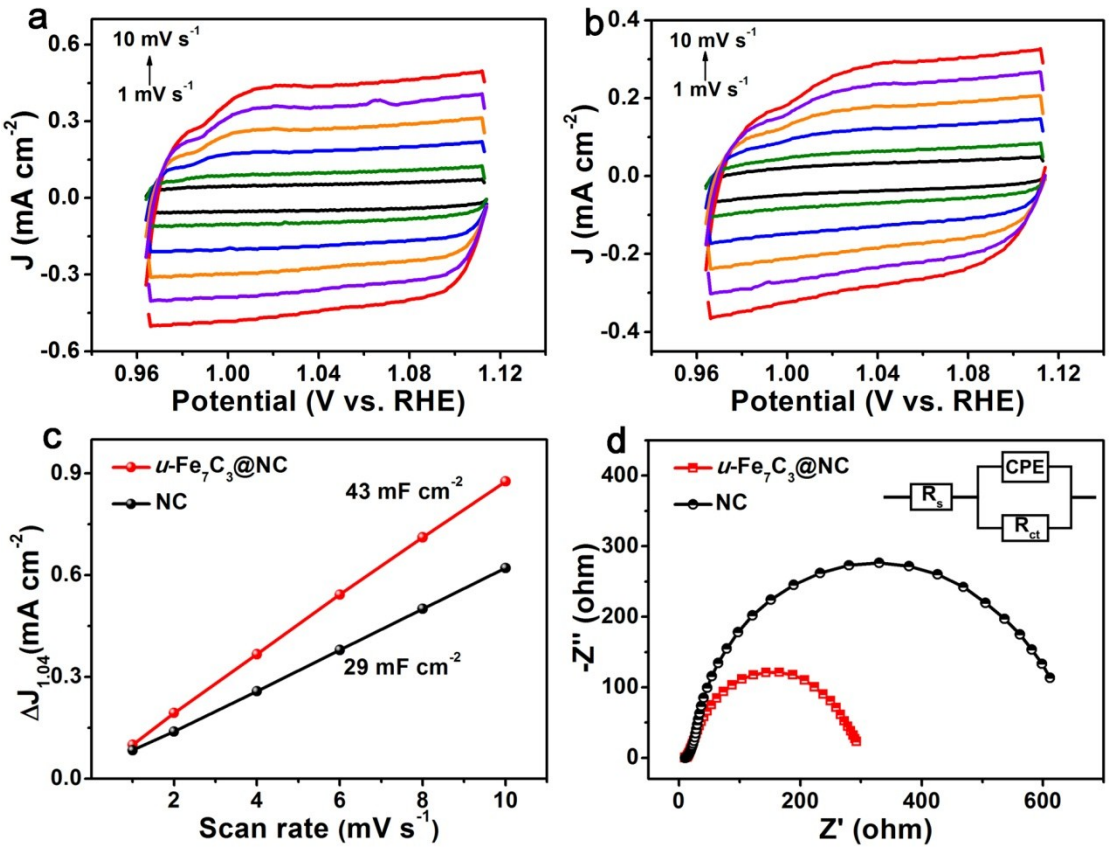


**Fig. S12** CV curves of (a) *u*-$Fe_7C_3$@NC and (b) NC in 0.10 M KOH at different scan rates of 1, 2, 4, 6, 8, and 10 mV $s^{-1}$, respectively. (c) The capacitive current density at 1.04 V as a function of scan rate for *u*-$Fe_7C_3$@NC and NC in 0.10 M KOH. (d) Nyquist plots of *u*-$Fe_7C_3$@NC and NC in 0.10 M KOH at open circuit potential.

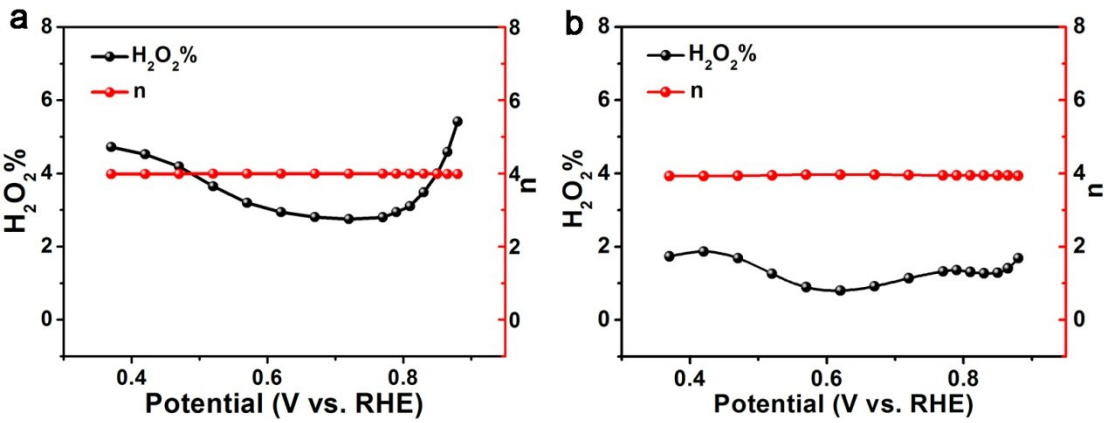


**Fig. S13** $H_2O_2$ yield ($H_2O_2$%) and electron transfer number (n) of (a) *u*-$Fe_7C_3$@NC and (b) the commercial Pt/C in $O_2$-saturated 0.10 M KOH solution.

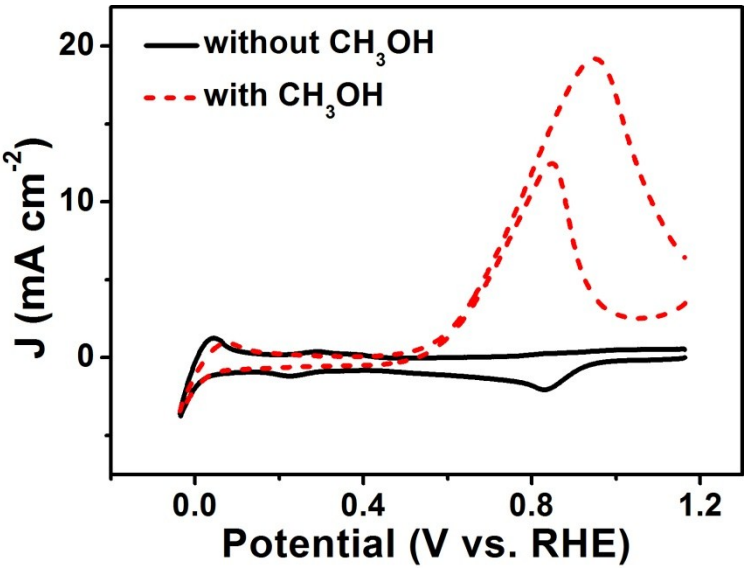


**Fig. S14** CVs of the commercial Pt/C in $O_2$-saturated 0.10 M KOH without and with 1.0 M $CH_3OH$ at a scan rate of 50 mV $s^{-1}$.

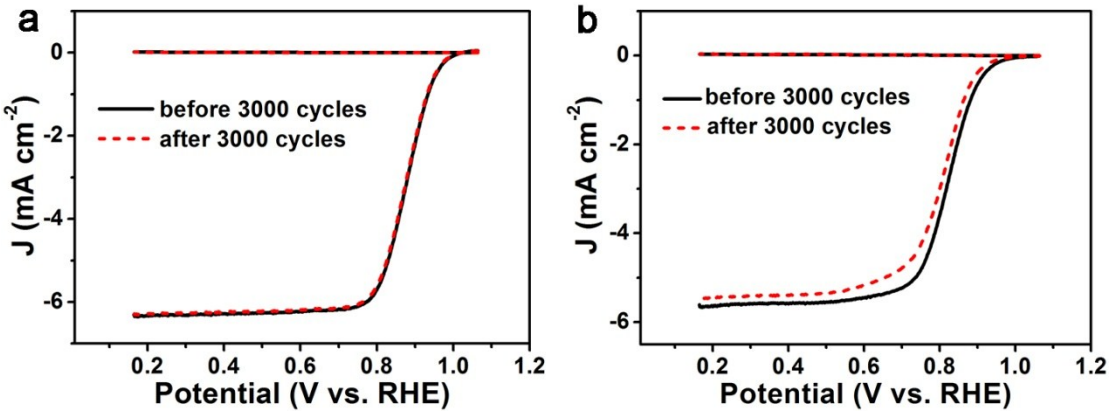


**Fig. S15** RRDE curves of (a) *u*-$Fe_7C_3$@NC and (b) Pt/C in $O_2$-saturated 0.10 M KOH before and after 3000 cycles.

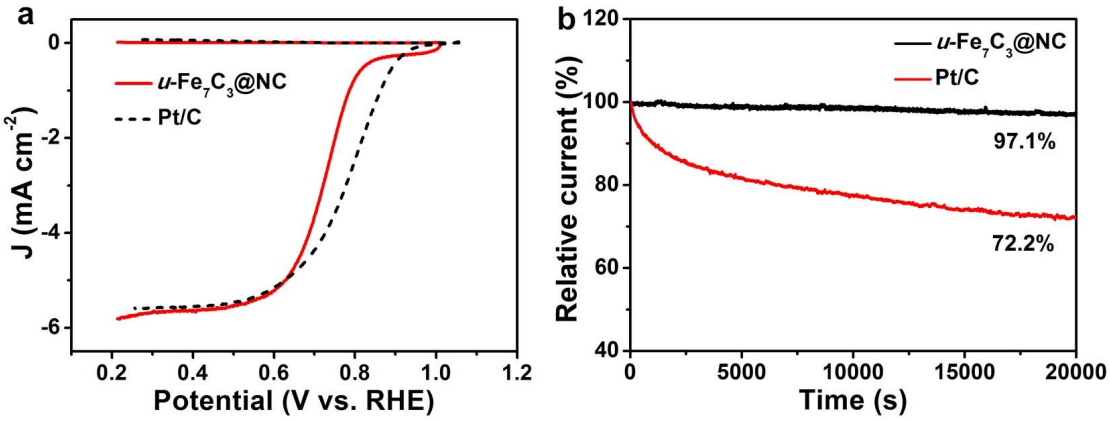


**Fig. S16** (a) RRDE voltammograms of *u*-$Fe_7C_3$@NC (0.50 M $H_2SO_4$) and Pt/C (0.10 M $HClO_4$) in $O_2$-saturated acidic solution. The scan rate is 5 mV $s^{-1}$ and the rotation rate is 1600 rpm. (b) Chronoamperometric curves of *u*-$Fe_7C_3$@NC (0.50 M $H_2SO_4$) and Pt/C (0.10 M $HClO_4$) in acidic solution.

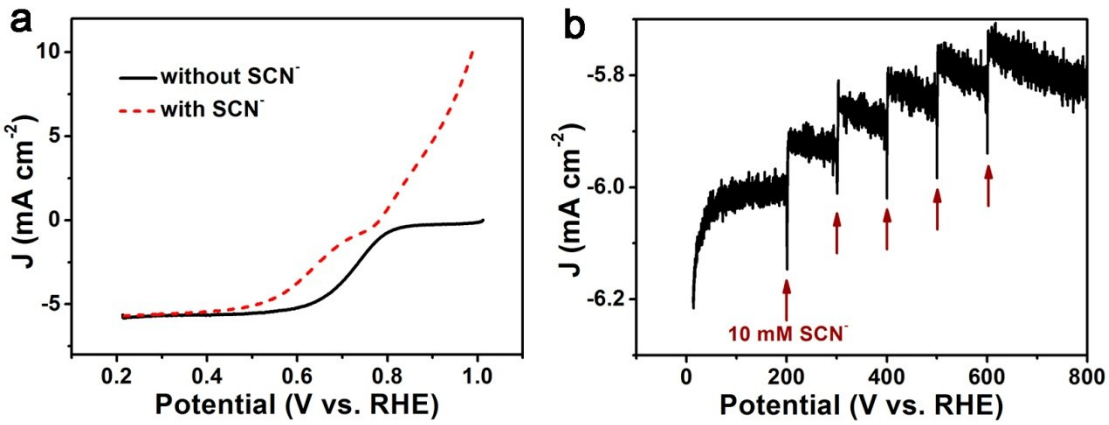


**Fig. S17** (a) LSV curves of *u*-$Fe_7C_3$@NC for ORR with or without 10 mM $SCN^-$ in 0.50 M $H_2SO_4$. (b) i-t curve of *u*-$Fe_7C_3$@NC for ORR with addition of $SCN^-$ in 0.50 M $H_2SO_4$.


**Fig. S18** Photograph of the Zn-air battery employing the commercial cathode, giving an open-circuit potential of 1.364 V.

**Table S1.** Atomic composition of *u*-$Fe_7C_3$@NC and NC obtained from XPS.

| Sample | Atomic composition (%) | | | | |
|---|---|---|---|---|---|
| | C | N | O | Fe | Zn |
| *u*-$Fe_7C_3$@NC | 85.02 | 2.87 | 11.8 | 0.29 | 0.02 |
| NC | 87.63 | 4.61 | 7.11 | 0 | 0.02 |

**Table S2.** Comparison of the ORR activity of *u*-$Fe_7C_3$@NC and reported iron carbides catalysts (The activity of catalysts was measured by LSV in 0.10 M KOH).

| Catalyst | $E_{1/2}$ (half-wave potential) (V) | $E_{onset}$ (onset potential) (V) | Ref. |
|---|---|---|---|
| GL-Fe/$Fe_5C_2$/NG-800 | 0.86 | 0.98 | [1] |
| PFA-Fe20-900-ALP | 0.83 | 0.87 | [2] |
| $Fe_3C$@Fe/N-graphene | 0.66 | 0.87 | [3] |
| Fe@Aza-PON | 0.84 | - | [4] |

| | | | |
|---|---|---|---|
| $Fe_3C$/b-NCNT | ~0.82 | 0.96 | [5] |
| FC10R | 0.812 | 0.835 | [6] |
| Fe-CZIF-800-10 | 0.83 | 0.982 | [7] |
| Fe@C-NG/NCNTs | 0.84 | 0.93 | [8] |
| $Fe_3C$/Fe@G-800 | 0.80 | 0.94 | [9] |
| LSMO-$Fe_3C$-NC | 0.85 | 0.98 | [10] |
| $Fe_3C$@N-CNT assemblies | 0.85 | 0.97 | [11] |
| $Fe_3C$/NCNTs/OBP-900 | 0.785 | 0.928 | [12] |
| Fe/N/C-800 | 0.84 | 0.954 | [13] |
| *u*-$Fe_7C_3$@NC | 0.88 | 0.98 | This work |

GL-Fe/$Fe_5C_2$/NG-800: graphene layers-wrapped Fe/$Fe_5C_2$ nanoparticles supported on N-doped graphene nanosheets

PFA-Fe20-900-ALP: carbonization of polyformamidine impregnated with 20 wt% of $FeCl_3$ at 900 °C

$Fe_3C$@Fe/N-graphene: mesoporous Fe/N-doped graphene with encapsulated $Fe_3C$ nanoparticles

Fe@Aza-PON: two-dimensional (2D) phenazine-based fused aromatic porous organic network

$Fe_3C$/b-NCNT: iron carbide ($Fe_3C$) nanoparticles encapsulated in N-doped bamboo-like carbon nanotubes

FC10R: Fe-$Fe_3C$ encapsulated in Fe-Nx enriched spheres of N-doped carbon nanotubes

Fe-CZIF-800-10: 3D interconnected hierarchical porous N-doped carbon with Fe/$Fe_3C$ nanoparticles via carbonization of ZIF-8 and potassium ferricyanide

Fe@C-NG/NCNTs: Fe/$Fe_3C$@C nanoparticles encapsulated in 3D N-doped graphene and bamboo-like CNTs

$Fe_3C$/Fe@G-800: graphene-coated iron and iron-carbide catalyst prepared at 800 °C

LSMO-$Fe_3C$-NC: three-components-integrated catalyst of $La_{0.5}Sr_{0.5}MnO_{3-\delta}$, $Fe_3C$ nanoparticles, and nitrogen-doped carbon

$Fe_3C$@N-CNT assemblies: iron carbide nanoparticle-embedded N-doped carbon nanotube assemblies supported by a porous N-doped carbon matrix

$Fe_3C$/NCNTs/OBP-900: $Fe_3C$ nanoparticles/N-doped carbon nanotubes/oxidized black pearl carbon

Fe/N/C-800: $Fe_3C$ dispersed on N-doped carbon by pyrolyzing the mixture of uric acid, iron (III) chloride anhydrous, and vulcan XC-72

**References**


1. E. Hu, X.-Y. Yu, F. Chen, Y. Wu, Y. Hu and X. W. D. Lou, *Advanced Energy Materials*, 2018, **8**, 1702476.
2. L. C. Pardo Pérez, N. R. Sahraie, J. Melke, P. Elsässer, D. Teschner, X. Huang, R. Kraehnert, R. J. White, S. Enthaler, P. Strasser and A. Fischer, *Advanced Functional Materials*, 2018, **28**, 1707551.
3. Y. Niu, X. Huang and W. Hu, *Journal of Power Sources*, 2016, **332**, 305-311.
4. S. J. Kim, J. Mahmood, C. Kim, G. F. Han, S. W. Kim, S. M. Jung, G. Zhu, J. J. De Yoreo, G. Kim and J. B. Baek, *Journal of the American Chemical Society*, 2018, **140**, 1737-1742.
5. A. Aijaz, J. Masa, C. Rosler, H. Antoni, R. A. Fischer, W. Schuhmann, and M. Muhler, *Chemistry - A European Journal*, 2017, **23**, 12125-12130.
6. R. Nandan, A. Gautam, S. Tripathi and K. K. Nanda, *Journal of Materials Chemistry A*, 2018, **6**, 8537-8548.
7. G. Li, J. Zhang, W. Li, K. Fan and C. Xu, *Nanoscale*, 2018, **10**, 9252-9260.
8. Q. Wang, Y. Lei, Z. Chen, N. Wu, Y. Wang, B. Wang and Y. Wang, *Journal of Materials Chemistry A*, 2018, **6**, 516-526.
9. A. Song, L. Cao, W. Yang, Y. Li, X. Qin and G. Shao, *ACS Sustainable Chemistry & Engineering*, 2018, **6**, 4890-4898.
10. B. Hua, M. Li and J.-L. Luo, *Nano Energy*, 2018, **49**, 117-125.
11. B. Y. Guan, L. Yu and X. W. Lou, *Energy & Environmental Science*, 2016, **9**, 3092-3096.
12. J. Zhu, M. Xiao, C. Liu, J. Ge, J. St-Pierre and W. Xing, *Journal of Materials Chemistry A*, 2015, **3**, 21451-21459.
13. J. Ma, D. Xiao, C. L. Chen, Q. Luo, Y. Yu, J. Zhou, C. Guo, K. Li, J. Ma, L. Zheng and X. Zuo, *Journal of Power Sources*, 2018, **378**, 491-498.